

Double-deconvolution method for the separation of thermalised emissions from chromium-doped lanthanum gallate and its potential in luminescence-based thermometry

Abbi L. Mullins^a, Aleksandar Ćirić^{*b}, Zoran Ristić^b, J. A. Gareth Williams^a, Ivana Radosavljević Evans^a, Miroslav D. Dramićanin^b

^aDepartment of Chemistry, Durham University, Durham DH1 3LE, UK

^bCentre of Excellence for Photoconversion, Vinča Institute of Nuclear Sciences – National Institute of the Republic of Serbia, University of Belgrade, P.O. Box 522, Belgrade 11001, Serbia

*Corresponding author email: aleksandar.ciric@ff.bg.ac.rs

Abstract

A series of $\text{LaGa}_{1-x}\text{O}_3:\text{Cr}^{3+}_x$ phosphors ($x = 0.002, 0.005, 0.01, 0.02, 0.04$) were synthesised by solid-state reaction and structurally characterised by Rietveld refinement from powder X-ray diffraction data. Amongst the five compounds, that with $x = 0.01$ exhibited the highest photoluminescence quantum yield at room temperature, those with higher doping levels probably suffering from self-quenching of the luminescence. This compound was selected for study of the temperature-dependence of the optical properties. The emission spectra recorded over the range 300–600 K reveal distinct features: a broad band that initially increases with temperature, attributed to fluorescence from the $^4\text{T}_2$ excited state, and a series of sharp peaks that monotonically decline with temperature, attributed to phosphorescence from the ^2E . The thermometry capabilities of $\text{LaGa}_{0.99}\text{O}_3:\text{Cr}_{0.01}$ were probed by the luminescence intensity ratio (LIR) method using the broad $^4\text{T}_2$ band relative to the sharp ^2E peaks. To overcome the difficulties associated with the significant overlap of the broad and sharp emissions of Cr^{3+} , a novel method was applied in which the deconvolution of broad peaks was performed in two steps, by fitting the broad bands to the curve sections without the sharp peaks. The ratio of the deconvoluted $^4\text{T}_2$ and ^2E intensities gave an excellent fit to the Boltzmann distribution, with an energy gap between them of 2172 cm^{-1} . The high relative sensitivity at room temperature of ca. $2.5\% \text{ K}^{-1}$ demonstrates very good potential of $\text{LaGa}_{0.99}\text{O}_3:\text{Cr}_{0.01}$ for thermometry in the first biological window of transparency, relevant for *in vivo* biomedical applications.

Keywords: deconvolution; luminescence thermometry; luminescence intensity ratio; LaGaO₃; Cr³⁺

1. Introduction

Lanthanum gallate LaGaO₃ (LGO) is a perovskite material that has potential in applications such as display screens, solid-oxide fuel cells, and luminescence thermometry [1–4]. Perovskite-type oxides adopt the general formula ABO₃, with cations A and B typically found in 12- and 6-coordinate sites, respectively. The stability and structural distortion of perovskites can be evaluated by Goldschmidt’s tolerance factor, t [5]:

$$t = \frac{r_A + r_O}{\sqrt{2}(r_B + r_O)} \quad (1)$$

where r_A , r_B , and r_O are the ionic radii of a 12-coordinate A cation, a 6-coordinate B cation, and a 2-coordinate oxide ion, respectively. An ideal perovskite has a Goldschmidt tolerance of $t \sim 1.0$ and adopts a cubic crystal structure. For LaGaO₃, $t = 0.973$. The material adopts an orthorhombic crystal structure in space group $Pnma$ (no. 62), with La³⁺ ions occupying Wyckoff site 4c with site symmetry m and Ga³⁺ on site 4a with site symmetry $\bar{1}$. In the crystal structure of LGO[6] (Figure 1), the BO₆ octahedra are tilted due to the La³⁺ ion in the central cavity being smaller than ideal. This causes a shortening of some of the La–O bonds at the expense of others, a change in the coordination number of La³⁺ from 12 to 8, and a lowering of the symmetry from cubic to orthorhombic. The octahedral tilting in LGO can be described by Glazer notation $a^+ b^- b^-/a^+ a^- a^-$ [7,8].

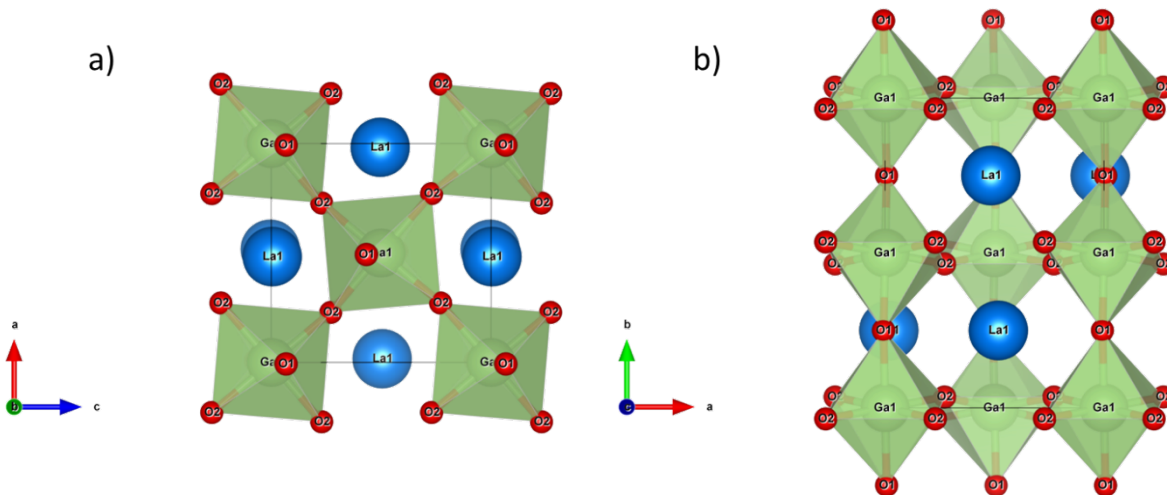


Figure 1. The structure of LGO (a) in the *ac* plane, showing the tilted GaO_6 octahedra, (b) in the *ab* plane, showing the corner-sharing cages of GaO_6 and the La^{3+} ions within the cavities. Green polyhedra represent GaO_6 groups, blue spheres represent La^{3+} ions and red spheres O^{2-} ions.

The Cr^{3+} ion has been frequently used as an activator for luminescence thermometry as it offers high emission intensity when in an appropriate environment with excellent thermal responses, allowing for highly sensitive temperature sensing [9–14]. The most frequently employed luminescence thermometric method is the Luminescence Intensity Ratio (LIR; often also known as fluorescence intensity ratio or FIR). For Cr^{3+} in strong crystal fields at cryogenic temperatures, the LIR of $R_{1,2}$ lines of the 2E state can be used for temperature sensing [15]. At room temperature, emission from the energetically proximate 4T_2 level starts to appear, increasing at the expense of the 2E level according to the Boltzmann law, until both emissions eventually decline due to temperature quenching. The ratio of integrated intensities of energetically higher ${}^4T_2 \rightarrow {}^4A_2$ emission to the lower ${}^2E \rightarrow {}^4A_2$ follows the Boltzmann distribution [16]:

$$LIR = \frac{I({}^4T_2)}{I({}^2E)} = B \exp\left(-\frac{\Delta E}{kT}\right) \quad (2)$$

where B is a temperature-invariant constant. ΔE in Eq. 2 usually underestimates the spectroscopically derived gap, since the Boltzmann fit only provides information on the energy difference between the zero-phonon energy of the lower excited state and the crossover point to the potential energy surface of the higher excited level. Figures of merit in luminescence thermometry – the absolute and relative sensitivity, S_a and S_r , respectively – are given for the LIR method by [17,18]:

$$S_a [K^{-1}] = \left| \frac{\partial LIR}{\partial T} \right|, S_r [\%K^{-1}] = \frac{S_a}{LIR} \quad (3)$$

The most important figure of merit for practical application of thermometers is the temperature resolution, which can be estimated from the relative sensitivity by $\Delta T = \sigma_r / S_r$, where σ_r is the uncertainty of LIR given as the standard deviation. The repeatability of measurements is estimated by [19]:

$$R [\%] = \left(1 - \frac{\max(|\text{mean}(LIR) - LIR_i|)}{\text{mean}(LIR)} \right) \cdot 100\% \quad (4)$$

where i represents the measurement count.

The ${}^4T_2 \rightarrow {}^4A_2$ and ${}^2E \rightarrow {}^4A_2$ emissions in Cr^{3+} significantly overlap, making the application of Eq. 2 rather difficult. The most frequently employed method for intensity determination is to take the onset tail of the broad peak as the energetically higher emission, and the integral of the remainder as the energetically lower. However, we have demonstrated previously [20,21] that deconvolution of the Cr^{3+} emission bands leads to a considerable increase of sensitivity in comparison with estimating the integrated intensities of two areas separated at an arbitrarily chosen wavelength. Additionally, the LIR by separation at a chosen wavelength frequently deviates from the Boltzmann distribution, necessitating that an additional offset is introduced into Eq. 2 [22].

In this work, LGO-based phosphors with five different Cr^{3+} concentrations were prepared, and the material with the highest quantum yield was investigated further by variable-temperature luminescence measurements to assess its suitability for temperature sensing, specifically as a potential *in vivo* thermometer, with broad excitation possibilities and intense emission in the first biological window. To overcome the difficulties in extracting the intensities of the 4T_2 and 2E emissions due to the significant overlap of the sharp and broad emissions in LGO: Cr^{3+} , we investigated a novel method for their separation based on two consecutive deconvolutions to completely separate broad from sharp peaks. The intensities obtained in this way were used to determine the LIR and the potential of the material in luminescence thermometry.

2. Experimental

Polycrystalline $LaGa_{1-x}O_3:Cr_x^{3+}$ ($x = 0.002, 0.005, 0.01, 0.02, 0.04$) samples were synthesised by conventional solid-state method from stoichiometric quantities of reagents on a scale to give 2 g of the product. La_2O_3 powder (Aldrich, $\geq 99.99\%$) was pre-heated to $900^\circ C$ for 10 h to remove moisture. Dried La_2O_3 , Ga_2O_3 (Aldrich, $\geq 99.99\%$), and Cr_2O_3 (Aldrich, 99.9%) powders were weighed out and ground for approximately 30 minutes with an agate mortar and pestle until homogenous. The samples were pressed into 10 mm diameter pellets, placed into an alumina crucible with a lid, and sintered in a muffle furnace at $1200^\circ C$ in the air for 70 h with intermittent grinding.

Powder X-ray diffraction (PXRD) was used to monitor the progress of solid-state reactions and to determine the purity of the products. All measurements were carried out at room temperature on a Bruker AXS d8 Advance diffractometer utilising $CuK\alpha$ radiation and a Lynx-Eye detector. Patterns were recorded over a range of $10^\circ < 2\theta < 90^\circ$ with a step size of 0.02° and step time of

0.5 s. All patterns were analysed in TOPAS academic software by Rietveld fitting. [23,24] In a typical refinement, parameters refined included unit cell parameters a , b , and c , an overall isotropic atomic displacement parameter, zero point, background polynomial terms, and pseudo-Voigt peak shape function parameters.

The quantum yields of the samples were measured using a Quanta-phi F-3029 integrating sphere. The powdered samples were contained in Spectralon sample holders with quartz cover slips. The samples were excited using light from a 450 W xenon lamp after passage through a monochromator. Neutral density filters were used to record the scattered light at λ_{ex} from the sample relative to a blank. The excitation spectra were recorded using a Horiba Jobin Yvon Fluorolog-3 fluorescence spectrometer.

Temperature-dependent emission spectra were acquired using an Ocean Insight FX spectrometer, coupled to a bifurcated fiber-optic probe, as presented in Figure 2. A 473 nm laser was used as the excitation source, and the reflected light was eliminated with a 500 nm long-pass filter. The sample was heated by a custom-made heating stage [25].

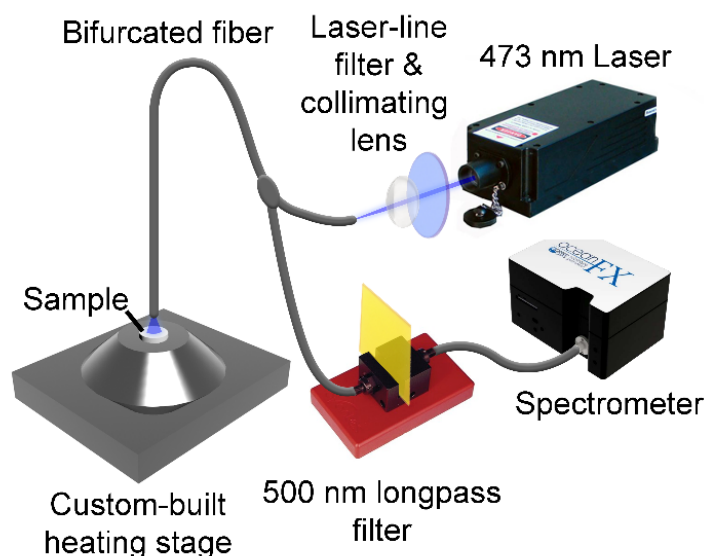


Figure 2. Experimental setup for thermometric measurements of $\text{LaGaO}_3:\text{Cr}^{3+}$.

3. Results & Discussion

3.1. Structural characterisation of $\text{LaGaO}_3:\text{Cr}^{3+}$

All PXRD patterns were fitted using an orthorhombic LaGaO_3 structural model in space group Pnma [26], adjusted for the present composition, with Cr^{3+} replacing some of Ga^{3+} ions. The unit cell parameters for $\text{LaGa}_{0.99}\text{O}_3:\text{Cr}_{0.01}$ are $a = 5.49237(9)$ Å, $b = 7.7744(1)$ Å, $c = 5.52457(8)$ Å, $V = 235.902(7)$ Å³. Figure 3 gives the final Rietveld fit obtained for $\text{LaGa}_{0.99}\text{O}_3:\text{Cr}_{0.01}$, showing excellent agreement between the observed and calculated data.

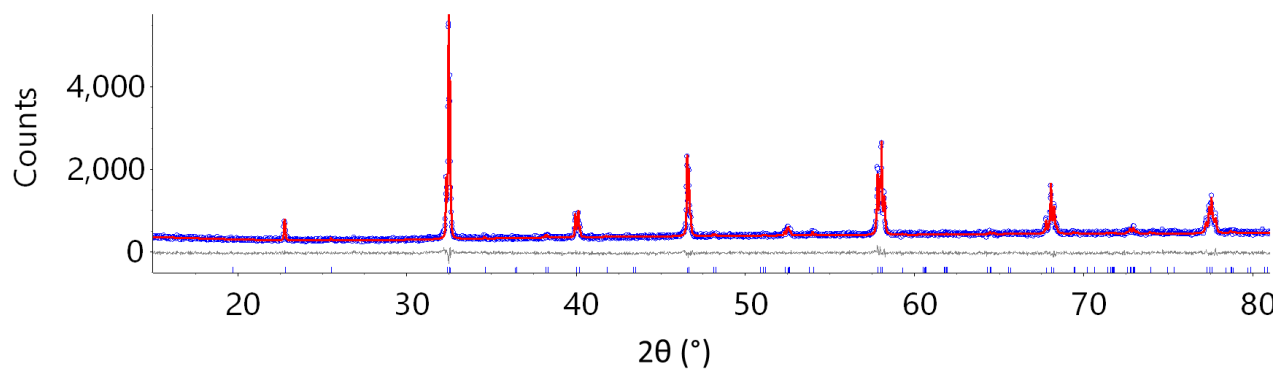


Figure 3: The final Rietveld fit obtained for $\text{LaGa}_{0.99}\text{O}_3:\text{Cr}_{0.01}$. The observed, calculated and difference curves are shown in blue, red and grey, respectively.

3.2. Photoluminescence analysis of $\text{LaGaO}_3:\text{Cr}^{3+}$

The sample with composition $\text{LaGa}_{0.99}\text{O}_3:\text{Cr}_{0.01}$ displayed the highest quantum yield, 8%, amongst the five samples with varying Cr^{3+} concentration. The superior performance over the compositions with $x > 0.01$ probably stems from inter-chromium quenching at the higher concentrations. This sample was therefore selected for further detailed analysis.

The photoluminescence excitation spectrum (

	Cr ³⁺ doping				
	0.002	0.005	0.01	0.02	0.04
QY (%)	6(2)	4(2)	8(2)	3(2)	<1(2)

Table 1: Quantum yields of the $\text{LaGa}_{1-x}\text{O}_3:\text{Cr}^{3+}_x$ ($x = 0.002, 0.005, 0.01, 0.02, 0.04$)

Figure 4a) features broad peaks typical for Cr^{3+} ions

in an octahedral environment, assigned to the spin-allowed ${}^4A_{2g} \rightarrow {}^4T_{2g}$ and ${}^4A_{2g} \rightarrow {}^4T_{1g}$ transitions. The positions of these bands are sensitive to the crystal field. In this material, they appear at 662 and 446 nm respectively, corresponding to energies of 16100 and 22400 cm^{-1} , respectively. The crystal field strength $10Dq$ (or Δ) and the Racah interelectronic repulsion parameter B can be determined from excitation or absorption spectra through reference to the Tanabe-Sugano diagram for d^3 ions in O_h symmetry [27], using the following well-established relationships [28]:

$$10Dq = E({}^4A_{2g} \rightarrow {}^4T_{2g}) \quad (5)$$

$$B = Dq \frac{\left(\frac{\Delta E}{Dq}\right)^2 - 10 \left(\frac{\Delta E}{Dq}\right)}{15 \left(\frac{\Delta E}{Dq} - 8\right)} \quad (6)$$

The calculated value of Dq/B is 2.54, which is indicative of a relatively strong-field environment for the Cr^{3+} ions. The crystal field strength $10Dq$ was calculated as 16070 cm^{-1} . The value of B was determined to be 630 cm^{-1} , which compares with that of 995 cm^{-1} for free Cr^{3+} ions [29]. The ratio, known as the nephelauxetic factor β , of 0.69 in this instance, provides a measure of the covalency of the Cr–O bonds. The value substantially < 1 is indicative of significant covalent character to the Cr–O bonds and substantial delocalisation of electron density over the oxide ligands [29].

The emission spectrum of $\text{LaGa}_{0.99}\text{O}_3:\text{Cr}_{0.01}$ excited at 473 nm at 300 K (Figure 4b) displays luminescence attributable only to the spin-forbidden ${}^2E \rightarrow {}^4A_2$ transition. The band is centred at 729 nm, corresponding to a 2E energy of 13700 cm^{-1} . The narrow bandwidth is typical of emission from the 2E state, whose energy is largely insensitive to Δ and hence to Cr–O vibrations. Stokes and anti-Stokes bands can be attributed to either side of the 2E peak [30]. Additionally, the peak at 739 nm is present due to Cr^{3+} - Cr^{3+} pairing known as an N-line [31]. At this temperature of 300 K, there is also a small proportion of accompanying broad-band emission to the high-energy side of the main band, attributable to the ${}^4T_2 \rightarrow {}^4A_2$ transition.

3.3. Luminescence thermometry of $\text{LaGa}_{0.99}\text{O}_3:\text{Cr}_{0.01}$

Temperature-dependent emission spectra (

Figure 4b) show that the broad ${}^4T_2 \rightarrow {}^4A_2$ emission, whose relative contribution increases with temperature, significantly overlaps with sharp emissions. To enable the reliable intensity determination needed for thermometry, the deconvolution of the emission spectrum was performed in two steps. In the first step, the tail of ${}^4T_2 \rightarrow {}^4A_2$ emission was fitted to the Jacobi transformation of the Gaussian function at the energy scale. After the first broad peak was subtracted from the spectrum, it was evident that the remaining peak is also comprised of sharp emissions and a broad peak. Figure 4b shows that the broad emission lies in the range from about 600 nm to 900 nm, and it increases with temperature up to ca. 450 K. This emission was firstly subtracted from the total emission by fitting the ends of the peak (from 600 nm to 650 nm, and from 800 nm to 900 nm) to the Gaussian function on the energy scale transformed by Jacobi transformation to the wavelength scale (broader, red-dashed line in Figure 4c). After this first subtraction, the existence of another, narrower, broad-band emission became evident, probably reflecting the local deviations from ideal octahedral symmetry. Analogously, this was subtracted from the remaining curve by fitting it to the area which did not contain any sharp peaks (650 nm to 700 nm; see narrower, red-dashed peak in

Figure 4c). After this second subtraction, only the sharp emissions remained (

Figure 4c green line). For the rapid and easy application of the double-deconvolution method, a MATLAB function has been created (which we have made freely available at www.omasgroup.org). The broad peaks, as they originate from the 4T_2 level, are summed up (

Figure 4c, red line). The integrated intensities of such deconvoluted emissions are given in Figure 4d.

The LIR of those two emissions, and the fitting to the Boltzmann equation, are given in

Figure 4e, giving a fitted energy separation of $\Delta E = 2172 \text{ cm}^{-1}$ and a quality of fit $R^2 = 0.994$. Without a clear separation of the ${}^4T_2 \rightarrow {}^4A_2$ and ${}^2E \rightarrow {}^4A_2$ transitions, the fit of LIR would not be possible without an additional parameter in the form of an offset to the Boltzmann distribution [22]. The quality of the fit shown in

Figure 4e demonstrates the validity of the double-deconvolution method. Absolute and relative sensitivities of the fitted LIR are presented in Figure 4f. $\text{LaGa}_{0.99}\text{O}_3:\text{Cr}_{0.01}$ shows the highest relative sensitivity of ca. $2.5\% \text{ K}^{-1}$ at room temperature. After 30 consecutive measurements at 300 K, the estimated relative uncertainty by our measuring setup is $\sigma_r = 0.13\%$, providing an excellent temperature resolution of $\Delta T = 0.05 \text{ K}$. The repeatability, estimated by Eq. 3, is 99.9%. Note that these outstanding results were obtained by using the high-quality equipment, by setting the maximum acquisition time and averaging each spectrum 100 times, which explains the low-temperature resolution value and the high repeatability. The typical relative uncertainty for LIR is about 1%, thus the best temperature resolution for a typical experimental setup is 0.4 K.

Similar LGO-based phosphors have been investigated previously for thermometric behaviour. Mondal *et al.* synthesised LGO: Cr^{3+} thermometers with a maximum LIR relative sensitivity of $2.07\% \text{ K}^{-1}$ at 150 K, and a temperature resolution of 0.24 K. [3] The LGO: Nd^{3+} thermometers reported by Back *et al.* had a maximum LIR relative sensitivity of $1.59\% \text{ K}^{-1}$ at 300

K and temperature resolution of ~ 1.0 K.[4] The Mn^{4+} ion, like Cr^{3+} , is a d^3 ion and has also been explored for luminescence thermometry, Li *et al.* having reported a $\text{LGO: Sm}^{3+}, \text{Mn}^{4+}$ material with a maximum relative sensitivity of $2.09\% \text{ K}^{-1}$ at 456 K [30]. Alongside Nd^{3+} , vanadium can be used in dual emission luminescence thermometers, taking advantage of its various oxidation states, as in $\text{LaGaO}_3\text{:V}, \text{Nd}^{3+}$ phosphors reported by Kniec *et al.* Relative sensitivities for the V^{5+} , V^{4+} , and V^{3+} -containing samples were, respectively, $1.0\% \text{ K}^{-1}$ at 268 K and 363 K ; $0.49\% \text{ K}^{-1}$ at -293 K ; and $1.44\% \text{ K}^{-1}$ at 348 K [31]. Compared with these literature examples, $\text{LaGa}_{0.99}\text{O}_3\text{:Cr}_{0.01}$ appears to show the highest LIR relative sensitivity for an LGO-based phosphor emitting within the $600\text{--}900 \text{ nm}$ wavelength region. This region of the spectrum corresponds to the 1st biological “window of transparency”, an important criterion for luminescence thermometers for use in biomedical applications [32].

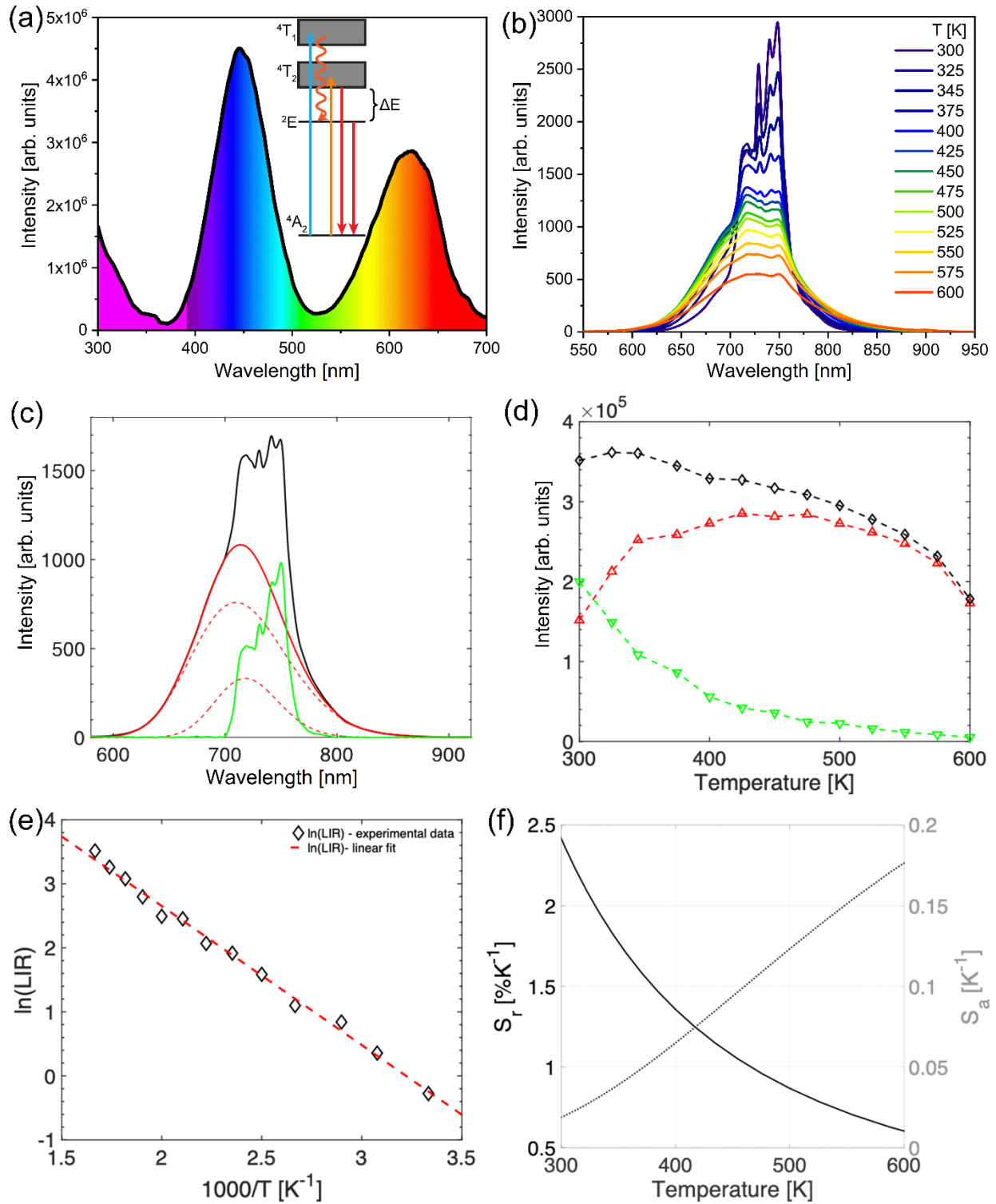


Figure 4. (a) Excitation spectrum of $\text{LaGa}_{0.99}\text{O}_3:\text{Cr}_{0.01}$ obtained by monitoring 750 nm emission, and the corresponding energy level diagram. (b) Emissions spectra of $\text{LaGa}_{0.99}\text{O}_3:\text{Cr}_{0.01}$ excited by 473 nm laser, at various temperatures. (c) The double-deconvolution method shown on an example of spectra at 375 K. Broad, subtracted emissions from the measured spectra (black

line) are given by red curves, and the remaining emission is given by green line. (d) Integrated intensities of total emissions (black), summed broad emissions (red), and sharp emissions (green). (e) LIR of broad emission (red) and sharp emissions (green) and fit to the Boltzmann relation. (f) Relative and absolute sensitivities were obtained from the fitted curve.

4. Conclusion

Orthorhombic perovskite-type $\text{LaGaO}_3:\text{Cr}^{3+}$ phosphors were successfully synthesised by a conventional solid-state method. Analysis of the room temperature excitation transitions of $\text{LaGa}_{0.99}\text{O}_3:\text{Cr}_{0.01}$ allowed for the crystal field splitting value Dq/B to be calculated as 2.54. This value is indicative of a strong crystal field at the Cr^{3+} centres, as confirmed by a sharp ${}^2\text{E}\rightarrow{}^4\text{A}_2$ R-line and a Cr^{3+} - Cr^{3+} pair N-line.

The $\text{LaGa}_{0.99}\text{O}_3:\text{Cr}_{0.01}$ sensor shows excellent performance in the physiological temperature range, specifically in the first biological window. By using time-gated detection, the excitation could be as well performed within the first biological window. The high signal intensity results in low uncertainties in measurement. Temperature resolution by this sensor is excellent and the novel double-deconvolution method provides high sensitivity. As the double-deconvolution method clearly separates the broad emissions due to the allowed transitions originating from the ${}^4\text{T}_2$ level from the sharp ${}^2\text{E}$ emissions, the thermometry closely follows the Boltzmann distribution without recourse to offsets.

Acknowledgments

All co-authors acknowledge funding by NATO grant SPS.MYP G5751 (The Optical Nose Grid for Large Indoor Area Explosives' Vapours Monitoring) and from the Ministry of Education, Science and Technological Development of the Republic of Serbia. ALM thanks EPSRC and Durham University for PhD funding.

References

- [1] X. Liu, J. Lin, Dy^{3+} - and Eu^{3+} -doped LaGaO_3 nanocrystalline phosphors for field emission displays, *J. Appl. Phys.* 100 (2006) 124306. <https://doi.org/10.1063/1.2400092>.
- [2] T. Ishihara, J. Tabuchi, S. Ishikawa, J. Yan, M. Enoki, H. Matsumoto, Recent progress in LaGaO_3 based solid electrolyte for intermediate temperature SOFCs, *Solid State Ionics.* 177 (2006) 1949–1953. <https://doi.org/10.1016/j.ssi.2006.01.044>.
- [3] A. Mondal, J. Manam, Structural, optical and temperature dependent photoluminescence

- properties of Cr³⁺-activated LaGaO₃ persistent phosphor for optical thermometry, *Ceram. Int.* 46 (2020) 23972–23984. <https://doi.org/10.1016/j.ceramint.2020.06.174>.
- [4] M. Back, J. Ueda, J. Xu, D. Murata, M.G. Brik, S. Tanabe, Ratiometric Luminescent Thermometers with a Customized Phase-Transition-Driven Fingerprint in Perovskite Oxides, *ACS Appl. Mater. Interfaces.* 11 (2019) 38937–38945. <https://doi.org/10.1021/acsami.9b13010>.
- [5] V.M. Goldschmidt, Die Gesetze der Krystallochemie, *Naturwissenschaften.* 14 (1926) 477–485. <https://doi.org/10.1007/BF01507527>.
- [6] K. Momma, F. Izumi, VESTA 3 for three-dimensional visualization of crystal, volumetric and morphology data, *J. Appl. Crystallogr.* 44 (2011) 1272–1276. <https://doi.org/10.1107/S0021889811038970>.
- [7] A.M. Glazer, The classification of tilted octahedra in perovskites, *Acta Crystallogr. Sect. B Struct. Crystallogr. Cryst. Chem.* 28 (1972) 3384–3392. <https://doi.org/10.1107/S0567740872007976>.
- [8] P.M. Woodward, Octahedral Tilting in Perovskites. II. Structure Stabilizing Forces, *Acta Crystallogr. Sect. B Struct. Sci.* 53 (1997) 44–66. <https://doi.org/10.1107/S0108768196012050>.
- [9] M. Back, J. Ueda, M.G. Brik, T. Lesniewski, M. Grinberg, S. Tanabe, Revisiting Cr³⁺-Doped Bi₂Ga₄O₉ Spectroscopy: Crystal Field Effect and Optical Thermometric Behavior of Near-Infrared-Emitting Singly-Activated Phosphors, *ACS Appl. Mater. Interfaces.* 10 (2018) 41512–41524. <https://doi.org/10.1021/acsami.8b15607>.
- [10] M. Back, J. Ueda, J. Xu, K. Asami, M.G. Brik, S. Tanabe, Effective Ratiometric Luminescent Thermal Sensor by Cr³⁺-Doped Mullite Bi₂Al₄O₉ with Robust and Reliable Performances, *Adv. Opt. Mater.* 8 (2020) 2000124. <https://doi.org/10.1002/adom.202000124>.
- [11] J. Ueda, M. Back, M.G. Brik, Y. Zhuang, M. Grinberg, S. Tanabe, Ratiometric optical thermometry using deep red luminescence from ⁴T₂ and ²E states of Cr³⁺ in ZnGa₂O₄ host, *Opt. Mater. (Amst).* 85 (2018) 510–516. <https://doi.org/10.1016/j.optmat.2018.09.013>.
- [12] M. Back, J. Ueda, M.G. Brik, S. Tanabe, Pushing the Limit of Boltzmann Distribution in Cr³⁺-Doped CaHfO₃ for Cryogenic Thermometry, *ACS Appl. Mater. Interfaces.* 12 (2020) 38325–38332. <https://doi.org/10.1021/acsami.0c08965>.

- [13] H. Aizawa, N. Ohishi, S. Ogawa, T. Katsumata, S. Komuro, T. Morikawa, E. Toba, Fabrication of ruby sensor probe for the fiber-optic thermometer using fluorescence decay, *Rev. Sci. Instrum.* 73 (2002) 3656–3658. <https://doi.org/10.1063/1.1505664>.
- [14] A. Ćirić, S. Stojadinović, Z. Ristić, Ž. Antić, M.D. Dramićanin, Temperature Sensing Using Ruby Coatings Created by Plasma Electrolytic Oxidation, *Sensors Actuators A Phys.* (2021) 112987. <https://doi.org/10.1016/j.sna.2021.112987>.
- [15] B.A. Weinstein, Ruby thermometer for cryobaric diamond-anvil cell, *Rev. Sci. Instrum.* 57 (1986) 910–913. <https://doi.org/10.1063/1.1138833>.
- [16] K. Elzbieciak, L. Marciniak, The Impact of Cr³⁺ Doping on Temperature Sensitivity Modulation in Cr³⁺ Doped and Cr³⁺, Nd³⁺ Co-doped Y₃Al₅O₁₂, Y₃Al₂Ga₃O₁₂, and Y₃Ga₅O₁₂ Nanothermometers, *Front. Chem.* 6 (2018). <https://doi.org/10.3389/fchem.2018.00424>.
- [17] G. Xiang, X. Liu, Q. Xia, S. Jiang, X. Zhou, L. Li, Y. Jin, L. Ma, X. Wang, J. Zhang, Deep-Tissue Temperature Sensing Realized in BaY₂O₄:Yb³⁺/Er³⁺ with Ultrahigh Sensitivity and Extremely Intense Red Upconversion Luminescence, *Inorg. Chem.* 59 (2020) 11054–11060. <https://doi.org/10.1021/acs.inorgchem.0c01543>.
- [18] G. Xiang, Q. Xia, X. Liu, Y. Wang, S. Jiang, L. Li, X. Zhou, L. Ma, X. Wang, J. Zhang, Upconversion nanoparticles modified by Cu₂S for photothermal therapy along with real-time optical thermometry, *Nanoscale.* 13 (2021) 7161–7168. <https://doi.org/10.1039/D0NR09115D>.
- [17] C.D.S. Brites, A. Millán, L.D. Carlos, Lanthanides in Luminescent Thermometry, in: J.-C. Bunzli, V.K. Pecharsky (Eds.), *Handb. Phys. Chem. Rare Earths*, Elsevier, 2016: pp. 339–427. <https://doi.org/10.1016/bs.hpre.2016.03.005>.
- [18] A. Ćirić, Z. Ristić, Ž. Antić, M.D. Dramićanin, An approximate deconvolution method for the luminescence intensity ratio calculations from overlapping emissions, *Phys. B Condens. Matter.* (2021) 413454. <https://doi.org/10.1016/j.physb.2021.413454>.
- [19] A. Ćirić, Z. Ristić, J. Periša, Ž. Antić, M.D. Dramićanin, MgAl₂O₄:Cr³⁺ luminescence thermometry probe in the physiological temperatures range, *Ceram. Int.* (2021). <https://doi.org/10.1016/j.ceramint.2021.06.131>.
- [20] S.A. Wade, S.F. Collins, G.W. Baxter, Fluorescence intensity ratio technique for optical fiber point temperature sensing, *J. Appl. Phys.* 94 (2003) 4743. <https://doi.org/10.1063/1.1606526>.
- [21] H.M. Rietveld, A profile refinement method for nuclear and magnetic structures, *J. Appl.*

- Crystallogr. 2 (1969) 65–71. <https://doi.org/10.1107/S0021889869006558>.
- [22] A.A. Coelho, J. Evans, I. Evans, A. Kern, S. Parsons, The TOPAS symbolic computation system, Powder Diffr. 26 (2011) S22–S25. <https://doi.org/10.1154/1.3661087>.
- [23] A. Ćirić, S. Stojadinović, M.D. Dramićanin, Custom-built thermometry apparatus and luminescence intensity ratio thermometry of $\text{ZrO}_2\text{:Eu}^{3+}$ and $\text{Nb}_2\text{O}_5\text{:Eu}^{3+}$, Meas. Sci. Technol. 30 (2019) 045001. <https://doi.org/10.1088/1361-6501/ab01b4>.
- [24] M. Lerch, H. Boysen, T. Hansen, High-temperature neutron scattering investigation of pure and doped lanthanum gallate, J. Phys. Chem. Solids. 62 (2001) 445–455. [https://doi.org/10.1016/S0022-3697\(00\)00078-0](https://doi.org/10.1016/S0022-3697(00)00078-0).
- [25] Y. Tanabe, S. Sugano, On the Absorption Spectra of Complex Ions II, J. Phys. Soc. Japan. 9 (1954) 766–779. <https://doi.org/10.1143/JPSJ.9.766>.
- [26] M. Back, E. Trave, J. Ueda, S. Tanabe, Ratiometric Optical Thermometer Based on Dual Near-Infrared Emission in Cr^{3+} -Doped Bismuth-Based Gallate Host, Chem. Mater. 28 (2016) 8347–8356. <https://doi.org/10.1021/acs.chemmater.6b03625>.
- [27] M.G. Brik, A.M. Srivastava, Comparative crystal field analysis of energy level schemes and nephelauxetic effect for Cr^{4+} , Cr^{3+} , and Mn^{4+} ions in $\text{Y}_2\text{Sn}_2\text{O}_7$ pyrochlore, Opt. Mater. (Amst). 35 (2013) 1251–1256. <https://doi.org/10.1016/j.optmat.2013.01.033>.
- [28] W. Ryba-Romanowski, S. Gołąb, G. Dominiak-Dzik, I. Sokólska, M. Berkowski, Optical study of chromium doped LaGaO_3 single crystal, J. Alloys Compd. 284 (1999) 22–26. [https://doi.org/10.1016/S0925-8388\(98\)00927-X](https://doi.org/10.1016/S0925-8388(98)00927-X).
- [29] W. Mikenda, A. Preisinger, N-lines in the luminescence spectra of Cr^{3+} -doped spinels (I) identification of N-lines, J. Lumin. 26 (1981) 53–66. [https://doi.org/10.1016/0022-2313\(81\)90169-1](https://doi.org/10.1016/0022-2313(81)90169-1).
- [30] Z. Li, X. Yu, T. Wang, S. Wang, L. Guo, Z. Cui, G. Yan, W. Feng, F. Zhao, J. Chen, X. Xu, J. Qiu, Highly sensitive optical thermometer of Sm^{3+} , Mn^{4+} activated LaGaO_3 phosphor for the regulated thermal behavior, J. Am. Ceram. Soc. 105 (2022) 2804–2812. <https://doi.org/10.1111/jace.18286>.
- [31] K. Kniec, L. Marciniak, Spectroscopic properties of $\text{LaGaO}_3\text{:V,Nd}^{3+}$ nanocrystals as a potential luminescent thermometer, Phys. Chem. Chem. Phys. 20 (2018) 21598–21606. <https://doi.org/10.1039/C8CP04080J>.

[32] A.M. Kaczmarek, M. Suta, H. Rijckaert, A. Abalymov, I. Van Driessche, A.G. Skirtach, A. Meijerink, P. Van Der Voort, Visible and NIR Upconverting Er³⁺-Yb³⁺ Luminescent Nanorattles and Other Hybrid PMO-Inorganic Structures for In Vivo Nanothermometry, *Adv. Funct. Mater.* 30 (2020) 2003101. <https://doi.org/10.1002/adfm.202003101>.